Dalton Transactions

Relativistic Modulation of Supramolecular Halogen/Copper Interactions and Phosphorescence in Cu(I) Pyrazolate Cyclotrimers

Journal:	*Dalton Transactions*
Manuscript ID	DT-ART-11-2022-003725.R1
Article Type:	Paper
Date Submitted by the Author:	13-Dec-2022
Complete List of Authors:	Lu, Zhou; University of North Texas, Chemistry; University of North Texas, Department of Chemistry Vanga, Mukundam; The University of Texas at Arlington, Chemistry and Biochemistry Li, Shan; University of North Texas, Chemistry Adebanjo, Joseph; University of North Texas, Chemistry Patterson, Monika; The University of Texas at Arlington, Chemistry and Biochemistry Dias, Rasika; The University of Texas at Arlington, Chemistry and Biochemistry Omary, Mohammad; University of North Texas, Chemistry

ARTICLE

Relativistic Modulation of Supramolecular Halogen/Copper Interactions and Phosphorescence in Cu(I) Pyrazolate Cyclotrimers

Received 00th January 20xx,
Accepted 00th January 20xx

DOI: 10.1039/x0xx00000x

Zhou Lu,[a] Mukundam Vanga,[b] Shan Li,[a] Joseph Adebanjo,[a] Monika R. Patterson,[b] H. V. Rasika Dias,*[b] and Mohammad A. Omary*[a]

Described herein is the synthesis, structure, and photophysics of the iodo-substituted cyclic, trinuclear copper(I) complex, $Cu_3[4\text{-I-}3,5\text{-}(CF_3)_2Pz]_3$ supported by a highly fluorinated pyrazolate and a detailed comparisons to its previously-reported 4-Br/4-Cl analogues. The crystal structure is stabilised by multiple supramolecular interactions of Cu_3···I and hydrogen/halogen bonding. The photophysical properties and supramolecular interactions are investigated experimentally/computationally for all three 4-halo complexes vs relativistic effects.

Introduction

Multinuclear copper(I) azolate complexes with interesting structures and luminescence properties have attracted significant attention.[1–3] Depending on the steric demands of the pyrazolate substitutes, planar trinuclear, saddle-shaped tetranuclear, and chain-like polynuclear copper complexes could be obtained displaying fascinating photophysical properties, including sensing abilities to temperature, solvent, concentration, and volatile organic compounds.[4–10] One representative class is that of cyclic trinuclear complexes (CTCs) of Cu(I)-pyrazolate, which could be easily synthesized through one-pot method and readily form supramolecular stacks through multiple types of interactions between the 9-membered ring planar moieties.[1,2,11–14] As reviewed in the literature, supramolecular interactions involved in CTCs include metallophilicity, π-acid/base interactions, hydrogen or halogen bonding, and host-guest interactions, some of which could reach interaction energies of ~10-20 kcal/mol alone or in combination.[1,2,11] With strong interaction energies, such supramolecular interactions are capable of influencing the intrinsic properties, creating abnormal phenomena such as charge-transfer, selective adsorption (including chemisorption), and sensitized luminescence of arene- ($^3\pi\pi^*$) or metal cluster- (^{3}MC) centred phosphorescence.[10,12,13,15–18]

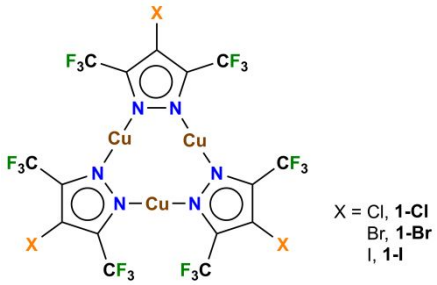

Scheme 1. Chemical structure of $Cu_3[4\text{-X-}3,5\text{-}(CF_3)_2Pz]_3$ (**1**).

Syntheses and crystal structures of highly-fluorinated, 4-Cl and 4-Br copper(I) CTCs, $Cu_3[4\text{-Cl-}3,5\text{-}(CF_3)_2Pz]_3$ (**1-Cl**) and $Cu_3[4\text{-Br-}3,5\text{-}(CF_3)_2Pz]_3$ (**1-Br**) were reported in our previous work (Scheme 1).[4] After fabricating **1-Cl** and **1-Br** materials into thin films, a proof-of-concept sensing application was tested upon exposure to vapours of benzene and its derivatives to exhibit reversible luminescence colour change over multiple cycles.[4] However, a detailed photophysical and theoretical investigation of the emissive state and radiative mechanism has not been studied to shed light on the design of such materials. In particular, tuning or modulating both the phosphorescence and its presumed underlying halogen---M interactions vs relativistic effects requires investigating the 4-I analogue (**1-I**, Scheme 1), as done herein (spin-orbit coupling constant, ξ = 587, 2460, and 5069 cm^{-1} for Cl (3p), Br (4p), and I (5p), respectively).[19]

Experimental Section

Materials and methods

All manipulations were carried out under an atmosphere of purified nitrogen using standard Schlenk techniques. Solvents were purchased from commercial sources, purified prior to use. Glassware was oven dried overnight at 150 °C. NMR spectra were acquired at 25 °C, on a JEOL Eclipse 500 spectrometer. ^{13}C NMR are referenced

[a] *Department of Chemistry, University of North Texas, 1155 Union Circle #305070, Denton, Texas 76203, United States. Email: omary@unt.edu*
[b] *Department of Chemistry and Biochemistry, The University of Texas at Arlington, Arlington, Texas 76019, United States. Email: dias@uta.edu*
Electronic Supplementary Information (ESI) available: characterization results, X-ray crystallography data, and computational. See DOI: 10.1039/x0xx00000x

to the solvent peak (^{13}C; $CDCl_3$ δ 77.16). ^{19}F NMR values were referenced to external $CFCl_3$. NMR solvents were purchased from Cambridge Isotopes Laboratories and used as received. Elemental analyses were performed using a Perkin-Elmer Model 2400 CHN analyser. Solid-state diffuse reflectance UV-vis characterizations were conducted on a Perkin-Elmer Lambda 900 UV/Vis/NIR spectrometer. Steady-state photoluminescence (PL) emission and excitation spectra were acquired with a PTI QuantaMaster Model QM-4 scanning spectrofluorometer with a 75-watt xenon arc lamp. A xenon flash lamp was used to acquire phosphorescence lifetime data in the microsecond regime. Solid samples were placed in a Suprasil quartz capillary tube inserted into a home-made liquid nitrogen cold finger with Suprasil quartz inner and outer tube irradiated components; this setup was used for PL measurements at both room temperature and 77 K. All reactants and reagents were purchased from commercial sources. Heating was accomplished by silicone oil bath. [4-I-3,5-$(CF_3)_2$Pz]H was synthesized using literature procedure.[20]

Synthesis procedure of Cu_3[4-I-3,5-$(CF_3)_2$Pz]$_3$ (1-I)

To a mixture of Cu_2O (0.25 g, 1.75 mmol) and [4-I-3,5-$(CF_3)_2$Pz]H (1.05 g, 3.18 mmol) in a 100 mL Schlenk were added anhydrous benzene (60 mL) and acetonitrile (5 drops) under inert atmosphere. The reaction mixture was then heated to reflux for 12 h. After cooling, the solution was filtered through a bed of celite to remove some insoluble material. The filtrate was collected, and the solvent was removed under reduced pressure to obtain Cu_3[4-I-3,5-$(CF_3)_2$Pz]$_3$ as white-coloured powder. It was then vacuum-dried at 80 °C for 5 h to remove trace solvent. X-ray quality crystals were grown from a solution of hot hexane. Yield: 1.1 g (88%) (based on the amount of pyrazole used). Anal. Calc. for $C_{15}Cu_3F_{18}I_3N_6$: C, 15.30; H, 0.00; N, 7.14; Found: C, 15.30; H, <0.10; N, 7.23. ^{19}F NMR (471 MHz, $CDCl_3$) δ = -60.54 (s, CF_3) ppm. ^{13}C NMR (126 MHz, $CDCl_3$) δ = 146.99 (q, $^2J_{C\text{-}F}$ = 34.8 Hz, C-3/C-5), 119.62 (q, $^1J_{C\text{-}F}$ = 271.1 Hz, CF_3), 54.88 (s, 4-C) ppm.

Crystallography

Single crystals of **1-I**, $C_{15}Cu_3F_{18}I_3N_6$ were grown by slow cooling of a solution in hot hexane. A suitable crystal was selected and mounted on a Bruker D8 Quest Photon 100 diffractometer. The crystal was kept at 100.00 K during data collection. Using Olex2,[21] the structure was solved with the SHELXT[22] structure solution program using Intrinsic Phasing and refined with the SHELXL[23] refinement package using Least Squares minimization. CCDC No.2204230 contains the supplementary crystallographic data for this paper. These data can be obtained free of charge via www.ccdc.cam.ac.uk/data_request/cif, or by emailing data_request@ccdc.cam.ac.uk, or by contacting The Cambridge Crystallographic Data Centre, 12 Union Road, Cambridge CB2 1EZ, UK; fax: +44 1223 336033.

Computational details

All the computational models were extracted from the single crystal structures and optimized in Gaussian 16 program software,[24] under the PBE0 level of theory incorporated with Def2-SVP basis sets.[25–27] Grimme's dispersion correction with Becke-Johnson damping (D3-BJ) was also adopted.[28,29] This methodology has been tested vs others by previous work on a similar CTC system, leading to better agreement with experimental results.[30] No imaginary frequencies were found to ensure the energies were in minima. Energy decomposition analysis (EDA) calculations were performed via the AMS 2020.103 software.[31] Functional PBE0 with D4 dispersion correction and all-electron TZ2P basis sets were adopted.[32,33] The fragments were designated and set as neutrally-charged, closed-shell states. The interaction energy ΔE = ΔE(entire model) – Σ[ΔE(fragment_i)]. The interaction energy (ΔE_{int}) is further decomposed into four terms, electrostatic energy (ΔE_{elstat}), Pauli repulsion (ΔE_{Pauli}), orbital interaction (ΔE_{OrbInt}), and dispersion correction (ΔE_{disp}).[34,35] Time-dependent density functional theory (TD-DFT) calculations were conducted in ORCA 4.2.1 program package in adopted PBE0 functional with Grimme's D3(BJ) dispersion correction.[36,37] A relativistically-recontracted all-electron DKH-Def2-TVZP(-f) basis set was used for C, N, Cl, F, and H atoms;[27] Sapporo-DKH3-TZP-2012 basis set was adopted for Cu, Br, and I atoms.[38] Relativistic effects were considered via 2nd order Douglas-Kroll-Hess (DKH2) method.[39,40] The electron density difference (EDD) maps and simulated absorption spectra were generated by Mulwiwfn 3.8 program.[41]

Results and discussion

Here we report the iodo-substituted Cu_3[4-I-3,5-$(CF_3)_2$Pz]$_3$ (**1-I**), which was synthesized through a one-pot method and isolated as a white powder, and a detailed experimental and computational study of its supramolecular and photophysical properties versus the 4-Cl and 4-Br analogues. The **1-I** has been fully characterized by NMR spectroscopy and X-ray diffraction techniques. Single crystals of **1-I** were grown from hot hexane. It crystalizes in monoclinic $P2_1/n$ (No. 14) space group. Detailed crystallographic data and selected bond lengths and angles are enclosed in ESI Tables S1 and S2. The asymmetric unit of **1-I** is shown in Fig. 1a, which has the aforementioned 9-membered-ring CTC structure. Three copper(I) atoms adopt linear coordination modes and are bridged by three pyrazolate ligands with N–Cu–N bond angles spanning 176.9(4)° to 179.8(3)°. The intra-trimer Cu–Cu distances range from 3.1559(16) to 3.3272(15) Å, all much longer than the summed van der Waals radii (r_{vdW}) of adjacent Cu atoms (2.80 Å). **1-I** adopts a trigonal bipyramidal-type stacking mode (Fig. 1b), consisting of I···Cu_3···I species with the halogen atom located above and below the metallacycle's plane at approximately the same distances (vs only one X···Cu_3 in the 4-Cl/4-Br analogues). This packing mode imparts slight puckering of trimer units, leading to ~20° dihedral angle deviation of Cu-Pz rings from planarity. Like its two **1-Cl**/**1-Br** analogues, **1-I** only has X···M and no M···M interactions. Hirshfeld surface analysis was conducted to find out the contacting fragment within the bipyramidal stack (Fig. 1c).[42] A noticeable point is the short F···F distances between two contacting **1-I** monomers (red spots in Fig. 1c), suggesting the existence of abundant F···F halogen contacts to stabilize the structure. White regions on the Hirshfeld surface in the Cu_3···I contact site also indicate that the Cu_3 plane to iodine atom

distances (3.2 Å) are close to the summed r_{vdW} of Cu and I atoms (3.38 Å).[43] To further investigate the supramolecular interaction, an independent gradient model based on the Hirshfeld partition (IGMH) was calculated for the optimized trimer-of-trimer model shown in Fig. 1d.[44] The surface reflects that the inter-trimer interactions are mainly comprised of non-covalent interactions, including F···F halogen bonding and π···π interactions between Pz rings. The strongest stabilization, however, is the Cu_3···I π-acid/Lewis base interaction, reflected by the blue regions on IGMH surface in Fig. 1d.

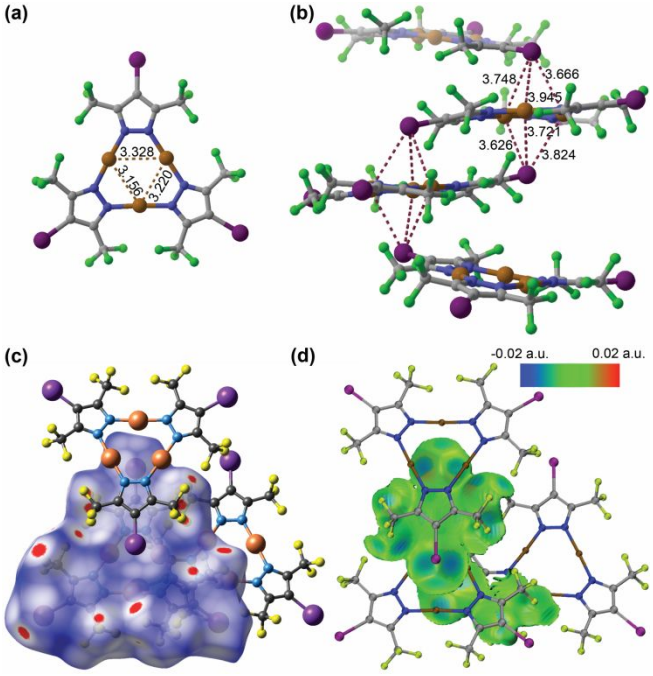

Fig. 1 (a) Molecular structure of **1-I**. (b) A view showing the inter-trimer I···Cu_3···I stacking mode. (c) Hirshfeld surface for **1-I** mapped with d_{norm} (-0.02 to +1.00) plotted on the promolecular surface. (d) *Sign*(λ_2)ρ coloured independent gradient model based on Hirshfeld partition (IGMH) δ_g^{inter} = 0.002 a.u. isosurfaces of a trimer of **1-I**, showing inter-trimer interactions. All distances labelled in the figure objects are in Å unit.

Energy decomposition analysis (EDA) calculations have also been performed for the three halogen-substituted **1-Cl**, **1-Br**, and **1-I** as well as the 4-unsubstituted $Cu_3[3,5\text{-}(CF_3)_2Pz]_3$ (as reference), as shown in Table 1. Both **1-Cl** and **1-Br** stack in the Cu_3···X trigonal pyramidal geometry rather than the I···Cu_3···I trigonal bipyramidal conformation in **1-I**. The single-capped stacking mode brings about lower interaction energy (ΔE) of -37.1 and -40.1 kcal/mol in **1-Cl** and **1-Br** models, respectively, vs -45.8 kcal/mol for **1-I** (based on trimer-of-trimer (TOT) models of all complexes at their crystallographic geometries preserving all Cu···X distances and association modes). To mimic the conformation in **1-Cl** and **1-Br**, hence have comparisons on an equal footing, we have investigated the dimer-of-trimer (DOT) mode of **1-I** structure with only one pair of Cu_3···I contact, attaining ΔE of -19.1 kcal/mol, close to half the values of -37.1 and -40.1 kcal/mol for TOT models of **1-Cl** and **1-Br**, respectively. At first sight, this result suggests that, under the same stacking mode, ΔE between monomers of **1** would not render significant additional stabilization for **1-I** vs **1-Cl** or **1-Br**. However, the stacking mode in **1-I** of two pairs of Cu_3···I contacts brings about significantly stronger interaction of -26.5 kcal/mol even in the single-capped model. Moreover, by breaking down the interaction energies, it can be noticed that the orbital interaction energy (ΔE_{OrbInt}) in **1-I** contributes to the overall attraction energy more than that in **1-Cl** and **1-Br**, such that a slight but significant, systematic increase is observed upon proceeding to the heavier halogen. Dispersion energy (ΔE_{disp}) still dominates the total attraction energy, similar to our previous finding in another supramolecular $[Au_3Pz_3]$@$[Ag_3Tz_3]$ charge transfer binary sytstem,[12] whereas the percentage of ΔE_{disp} in **1-I** is significantly smaller than that in **1-Cl** or **1-Br**. The change in ΔE_{OrbInt} and ΔE_{disp} is presumably caused by the significantly stronger relativistic effect of the heavier iodine atom and its filled $5p_z$ orbital upon interactions with the empty $4p_z$ orbitals of Cu atoms so as to impart greater orbital interaction, comparing to the Cl- and Br-analogues.[45] For reference, EDA in a 4-unsubstituted $\{Cu_3[3,5\text{-}(CF_3)_2Pz]_3\}_2$ dimer shows that, even though ΔE is stronger vs DOT models with one pair of Cu_3···I contact, the orbital interaction contribution thereof is still lower than that in *all models* of 4-halogen–Cu_3 analogues, suggesting that the halogen···metal (X···M) supramolecular interaction can, not only be comparable with, but, indeed, exceed metallophilicity (M···M).[46]

Table 1 Energy decomposition analyses (EDA) results of associating $Cu_3[4\text{-}X\text{-}3,5\text{-}(CF_3)_2Pz]_3$ (**1-X**) models vs X; model **1-H** = $Cu_3[3,5\text{-}(CF_3)_2Pz]_3$. (%) values = contributions to total attraction energy between trinuclear units. All units = kcal/mol. See Fig. S13 for model geometries.

Model	ΔE_{elstat}	ΔE_{Pauli}	ΔE_{OrbInt}	ΔE_{disp}	ΔE
[**1-Cl**]$_3$ (2*1Cu_3···Cl)	-12.8 (24%)	15.6	-7.8 (15%)	-32.0 (61%)	-37.1
[**1-Br**]$_3$ (2*1Cu_3···Br)	-12.5 (23%)	13.8	-9.3 (17%)	-32.0 (59%)	-40.1
[**1-I**]$_3$ (1Cu_3···I+2Cu_3'···I')	-30.5 (35%)	40.8	-17.5 (20%)	-38.6 (45%)	-45.8
[**1-I**]$_2$ (1Cu_3···I)	-9.7 (31%)	12.5	-5.8 (18%)	-16.1 (51%)	-19.1
[**1-I**]$_2$ (2Cu_3'···I')	-20.9 (38%)	28.0	-11.7 (21%)	-21.9 (40%)	-26.5
[**1-H**]$_2$ (1Cu···Cu)	-9.9 (28%)	12.1	-5.1 (14%)	-20.8 (58%)	-23.6

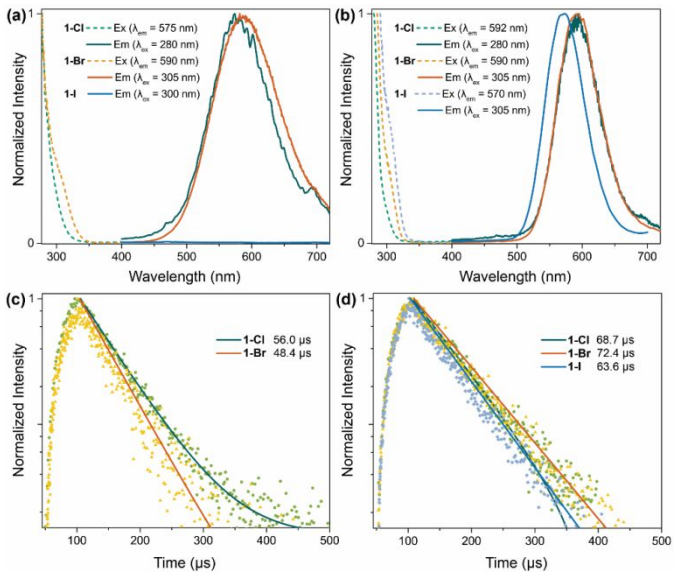

Fig. 2 Steady-state photoluminescence excitation and emission spectra of **1** solid at (a) room temperature and (b) 77 K. Emission decay curves of **1** solid at (c) room temperature and (d) 77 K.

We have further investigated the photoluminescence properties of **1-I** solid powder vs its two lighter halogenated analogues on equal footing. To ameliorate any possible influence of solvent residues and prevent the formation and/or co-crystallization of CTC-arene adducts, all solid powders were dried in a vacuum oven overnight before the photoluminescence measurements.[4] As shown in Fig. 2a, **1-I** is non-emissive under room temperature while **1-Cl** and **1-Br** exhibit yellow emissions centred around 575 and 590 nm, respectively. Excitation profiles of **1-Cl** and **1-Br** reveal a high-energy band below 280 nm, which is beyond the instrument's detection limit, together with an excitation shoulder near 300 nm. When cooling to 77 K, as depicted in Fig. 2b, **1-I** shows a bright emission peaked at 570 nm while the emissions of **1-Cl** and **1-Br** remain almost unchanged from their room temperature positions (albeit with a significant decrease of the full width at half maximum, FWHM, as expected due to decreased thermal broadening at cryogenic temperatures).[47] The emission lifetime profiles of the three **1** solids are recorded in Figs. 2c-2d. Fitted emission lifetimes are in the 60-μs range, revealing their phosphorescence nature. Comparing the absorption profiles of the three **1** complexes, a red shift could be observed for **1-I** with a peak centred around 375 nm under room temperature, whereas **1-Cl** and **1-Br** exhibit absorption peaks near 325 nm (Figs. S3-S5). Although the emission and lifetime properties of the three **1** complexes are similar, suggesting a similar origin of their emissive triplet excited states, the absorption and excitation bands suggest possibly different photophysical pathways in response to the distinct packing modes and interaction energies for **1-I** vs **1-Cl** or **1-Br**.

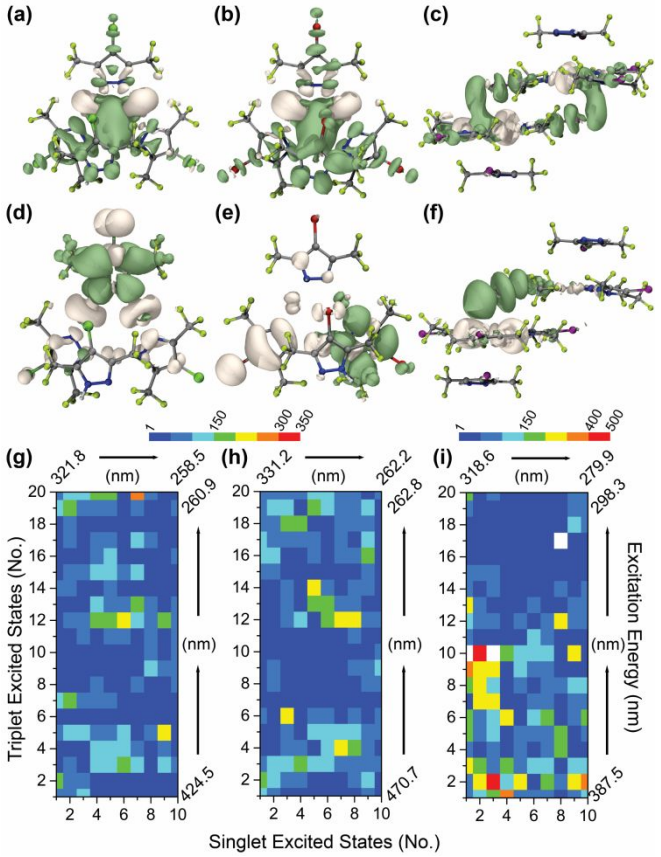

Fig. 3 Electron density difference (EDD) maps of the lowest-singlet excited states (S_1) of (a) **1-Cl**, (b) **1-Br**, and (c) **1-I**. EDD maps of the lowest-triplet excited states (T_1) of (d) **1-Cl**, (e) **1-Br**, and (f) **1-I**. White and green regions refer to the decrease and increase of electron density, respectively. Heatmaps of spin-orbit coupling matrix elements (SOCMEs, in cm^{-1}) between the 10 lowest S_n states and 20 lowest T_n states of (g) **1-Cl**, (h) **1-Br**, and (i) **1-I**; m and n are integral values ≥ 1.

To understand the photophysical processes in the three **1** adducts, time-dependent density functional theory (TD-DFT) calculations were conducted. Models of **1-Cl** and **1-Br** were constructed by a full Cu_3Pz_3 trimer and a neighbouring protonated ligand to preserve the Cu_3···X pyramidal geometry; for **1-I**, a head-to-tail DOT and two protonated ligands were modelled. All selected computational models were optimized in singlet (S_0) or triplet (T_1) multiplicities and no imaginary frequencies were found, ascertaining that the optimized structures represent minima. As the heavy-atom effect here significantly influences the phosphorescence and owing to the evidential Cu_3···X π-acid/Lewis base interactions, relativistic effects in spin-orbit coupling (SOC) calculations have been considered by adopting the 2nd-order Douglas–Kroll–Hess (DKH2) method to study the photophysical processes and obtain detailed information regarding triplet excited states (T_m).[39,40] First, simulated excitation spectra of all three **1** models are in good agreement with the experimental spectra (Figs. S3-S5, S9-S11). Figs. 3a-b show the electron density difference (EDD) maps of S_1 states of **1-Cl** and **1-Br** with a mixture of metal-centred (^{1}MC) and metal-to-ligand charge transfer (^{1}MLCT; L =

Pz ring) origin, both being the common intramolecular form in a monomeric CTC unit; electrons flow from the white to the green regions in EDD maps during the excitation process. However, **1-I** exhibits a mixture of ^{1}MC and through-space (intermolecular) ^{1}ML'CT/^{1}XM'CT, whereby the X (iodine) atoms from one CTC play an essential role in conjugating with the Cu_3 core centre from another CTC, due to a shorter I···Cu_3 contact distance (Fig. 3c). Second, EDD maps of the T_1 states of **1** have been generated and depicted in Figs. 3d-f. A through-space ^{3}ML'CT character dominates the **1-I** phosphorescence character much more clearly than that for **1-Cl** and **1-Br**, consistent with the above X-ray data and DFT modelling results thereof, all showing much stronger X···Cu intermolecular interactions in the iodo analogue. The through-space character therein is also consistent with the trigonal bipyramidal-type stacking mode and the stronger interaction energies for **1-I**. We have noticed that, in all theoretical models, the co-existing deprotonated ligands are not involved in the phosphorescence pathway, which is in sharp contrast to the luminescence properties of the Cu(I)/Ag(I)/Au(I) CTC-arene adducts or even simple mixtures.[1,4,10,15] This is speculated to arise from the weaker (Lewis) basicity of halogen-substituted pyrazoles versus π-electron-rich benzene and toluene. Thus, such electron-deficient CTCs are potential sensing (and possibly filtering/remediating) materials for π-rich molecules.

In order to describe the role of SOC on the luminescence properties, SOC matrix elements (SOCMEs) have been calculated to find the inter-system crossing (ISC) pathways and locate the singlet and triplet excited states (S_n and T_m) involved.[30] Heatmaps of SOCMEs between the first ten S_n and twenty T_m states are depicted in Figs. 3g-3i. Besides SOCME values, two more factors should be considered to find the ISC pathways: the small energy differences between possible S_n and T_m states and the large oscillator strength of initial photon-excited S_n states. From Figs. 3g-3h and Tables S3-S4, we can identify several possible ISC pathways for **1-Cl** and **1-Br**, classified as one low-lying from S_1 or S_2 to close-energy T_5, T_6, and/or T_7, and one relatively high-lying channels from S_4, S_5, and/or S_6 with a high oscillator strength to T_{12}, T_{13}, and/or T_{14} states. For **1-I**, in contrast, profiles of the singlet excited states are different such that low-lying S_n states also exhibit large oscillator strengths and are more likely reckoned as the only starting states for ISC, as shown in Fig. 3i and Table S5. The high-lying S_n states involved in the photophysical pathways for **1-Cl** and **1-Br** also correspond to the high-energy absorption bands found in the solid-state UV-vis absorption spectra, which contrasts the situation for **1-I** that exhibits lower-energy absorption bands resulting from low-lying S_n states. These data suggest that **1-Cl** and **1-Br** have more accessible ISC pathways through high-lying singlet excited states, whereas only low-lying and less-efficient ISC pathways could be found in **1-I**, which are unfavourable through thermal equilibrium. As a consequence, no emission was observed for **1-I** under room temperature. Thus, the stronger SOC in **1-I** involves accelerated non-radiative (k_{nr}) as opposed to radiative (k_r) rate constants, explaining the experimental absence of room temperature phosphorescence in this compound vs its two lighter congeners **1-Cl**/**1-Br**. A similar situation was found for the internal heavy-atom effect in 1-halonapthalene binary adducts with a perfluorinated Hg(II) CTC by the Gabbaï/Omary team.[48]

Conclusions

In conclusion, we have synthesized the highly fluorinated and iodine-substituted Cu_3[4-I-3,5-$(CF_3)_2$Pz]$_3$ CTC and investigated its (supra)molecular structure and photophysical properties experimentally and theoretically with a detailed comparison to its 4-Cl/4-Br analogues. Through structural analysis and DFT calculations, the major stabilization of the crystals is found to be the I···Cu_3···I double-capped interactions, which are stronger than those of the single-capped Cl/Br···Cu_3 interactions found in analogues **1-Cl** and **1-Br**. Photoluminescence studies of the solid samples of three heavier (than F) 4-halogen-substituted **1** compounds have been conducted experimentally, supported by TD-DFT computations with explicit SOC treatment in order to understand the excited state assignment. These results reveal that the unique I···Cu_3···I double-capped conformation in **1-I** gives rise to an intertrimer through-space ^{3}ML'CT phosphorescent state, much more clearly manifested than analogous models for the single-capped **1-Cl/Br** congeners. Expansion studies on analogous Ag(I) and Au(I) 4-I/X-substituted CTCs remains to be explored, as well as their applications in sensing/remediation of arenes and other environmental pollutants.

Conflicts of interest

There are no conflicts to declare.

Acknowledgements

This work has been supported by Welch Foundation (B-1542; M.A.O.) and the National Science Foundation under grant numbers CHE-1413641 (M.A.O.) and CHE-1954456 (H.V.R.D.). The authors also acknowledge the support by the National Science Foundation to the University of North Texas through grant CHE-1531468 for high-performance computing resources.

Notes and references

1 J. Zheng, Z. Lu, K. Wu, G.-H. Ning and D. Li, *Chem. Rev.*, 2020, **120**, 9675–9742.
2 R. Galassi, M. A. Rawashdeh-Omary, H. V. R. Dias and M. A. Omary, *Comments Inorg. Chem.*, 2019, **39**, 287–348.
3 J.-P. Zhang, Y.-B. Zhang, J.-B. Lin and X.-M. Chen, *Chem. Rev.*, 2011, **112**, 1001–1033.
4 C. V. Hettiarachchi, M. A. Rawashdeh-Omary, D. Korir, J. Kohistani, M. Yousufuddin and H. V. R. Dias, *Inorg. Chem.*, 2013, **52**, 13576–13583.
5 N. B. Jayaratna, I. I. Gerus, R. V. Mironets, P. K. Mykhailiuk, M. Yousufuddin and H. V. R. Dias, *Inorg. Chem.*, 2013, **52**, 1691–1693.
6 H. V. R. Dias, H. V. K. Diyabalanage, M. M. Ghimire, J. M.

Hudson, D. Parasar, C. S. P. Gamage, S. Li and M. A. Omary, *Dalton Trans.*, 2019, **48**, 14979–14983.
7 M. Patterson and H. V. R. Dias, *Dalton Trans.*, 2022, **51**, 375–383.
8 Y. Watanabe, B. M. Washer, M. Zeller, S. Savikhin, L. V. Slipchenko and A. Wei, *J. Am. Chem. Soc.*, 2022, **144**, 10186–10192.
9 N. Masciocchi, M. Moret, P. Cairati, A. Sironi, G. A. Ardizzoia and G. L. Monica, *J. Am. Chem. Soc.*, 1994, **116**, 7668–7676.
10 S.-Z. Zhan, F. Ding, X.-W. Liu, G.-H. Zhang, J. Zheng and D. Li, *Inorg. Chem.*, 2019, **58**, 12516–12520.
11 J. Zheng, H. Yang, M. Xie and D. Li, *Chem. Commun.*, 2019, **55**, 7134–7146.
12 Z. Lu, B. Chilukuri, C. Yang, A.-M. Rawashdeh, R. K. K. Arvapally, S. Tekarli, X. Wang, C. Cardenas, T. R. Cundari and M. A. Omary, *Chem. Sci.*, 2020, **11**, 11179–11188.
13 Z. Lu, Y.-J. Yang, W.-X. Ni, M. Li, Y. Zhao, Y.-L. Huang, D. Luo, X. Wang, M. A. Omary and D. Li, *Chem. Sci.*, 2021, **12**, 702–708.
14 R. Galassi, M. M. Ghimire, B. M. Otten, S. Ricci, R. N. McDougald Jr., R. M. Almotawa, D. Alhmoud, J. F. Ivy, A.-M. M. Rawashdeh, V. N. Nesterov, E. W. Reinheimer, L. M. Daniels, A. Burini and M. A. Omary, *Proc. Natl. Acad. Sci. U. S. A.*, 2017, **114**, E5042–E5051.
15 M. M. Ghimire, O. C. Simon, L. M. Harris, A. Appiah, R. M. Mitch, V. N. Nesterov, A. Macchioni, C. Zuccaccia, H. Rabaâ, R. Galassi and M. A. Omary, *Inorg. Chem.*, 2019, **58**, 15303–15319.
16 R. Liu, W.-H. Zhang, D. Wei, J.-H. Chen and G. Yang, *Dalton Trans.*, 2019, **48**, 16162–16166.
17 M. Xie, X.-R. Chen, K. Wu, Z. Lu, K. Wang, N. Li, R.-J. Wei, S.-Z. Zhan, G.-H. Ning, B. Zou and D. Li, *Chem. Sci.*, 2021, **12**, 4425–4431.
18 N. B. Jayaratna, M. G. Cowan, D. Parasar, H. H. Funke, J. Reibenspies, P. K. Mykhailiuk, O. Artamonov, R. D. Noble and H. V. R. Dias, *Angew. Chem., Int. Ed.*, 2018, **57**, 16442–16446.
19 S. Fraga, J. Karwowski and K. M. S. Saxena, *Handbook of Atomic Data*, Elsevier, 1976, vol. 5.
20 A. Maspero, G. B. Giovenzana, D. Monticelli, S. Tagliapietra, G. Palmisano and A. Penoni, *J. Fluorine Chem.*, 2012, 139, 52–56.
21 O. V. Dolomanov, L. J. Bourhis, R. J. Gildea, J. A. K. Howard and H. Puschmann, *J. Appl. Crystallogr.*, 2009, **42**, 339–341.
22 G. M. Sheldrick, *Acta Crystallogr., Sect. A: Found. Adv.*, 2015, **A71**, 3–8.
23 G. M. Sheldrick, *Acta Crystallogr., Sect. C: Struct. Chem.*, 2015, **C71**, 3–8.
24 M. J. Frisch, G. W. Trucks, H. B. Schlegel, G. E. Scuseria, M. A. Robb, J. R. Cheeseman, G. Scalmani, V. Barone, G. A. Petersson, H. Nakatsuji, X. Li, M. Caricato, A. V. Marenich, J. Bloino, B. G. Janesko, R. Gomperts, B. Mennucci, H. P. Hratchian, J. V. Ortiz, A. F. Izmaylov, J. L. Sonnenberg, D. Williams-Young, F. Ding, F. Lipparini, F. Egidi, J. Goings, B. Peng, A. Petrone, T. Henderson, D. Ranasinghe, V. G. Zakrzewski, J. Gao, N. Rega, G. Zheng, W. Liang, M. Hada, M. Ehara, K. Toyato, R. Fukuda, J. Hasegawa, M. Ishida, T. Nakajima, Y. Honda, O. Kitao, H. Nakai, T. Vreven, K. Throssell, J. A. Montgomery Jr., J. E. Peralta, F. Ogliaro, M. J. Bearpark, J. J. Heyd, E. N. Brothers, K. N. Kudin, V. N. Staroverov, T. A. Keith, R. Kobayashi, J. Normand, K. Raghavachari, A. P. Rendell, J. C. Burant, S. S. Iyengar, J. Tomasi, M. Cossi, J. M. Millam, M. Klene, C. Adamo, R. Cammi, J. W. Ochterski, R. L. Martin, K. Morokuma, O. Farkas, J. B. Foresman and D. J. Fox, *Gaussian 16*, 2016.
25 J. P. Perdew, K. Burke and M. Ernzerhof, *Phys. Rev. Lett.*, 1996, **77**, 3865–3868.
26 J. P. Perdew, K. Burke and M. Ernzerhof, *Phys. Rev. Lett.*, 1997, **78**, 1396–1396.
27 F. Weigend and R. Ahlrichs, *Phys. Chem. Chem. Phys.*, 2005, **7**, 3297–3305.
28 S. Grimme, *J. Comput. Chem.*, 2006, **27**, 1787–1799.
29 S. Grimme, S. Ehrlich and L. Goerigk, *J. Comput. Chem.*, 2011, **32**, 1456–1465.
30 L.-R. Xing, Z. Lu, M. Li, J. Zheng and D. Li, *J. Phys. Chem. Lett.*, 2020, **11**, 2067–2073.
31 G. te Velde, F. M. Bickelhaupt, E. J. Baerends, C. F. Guerra, S. J. A. van Gisbergen, J. G. Snijders and T. Ziegler, *J. Comput. Chem.*, 2001, **22**, 931–967.
32 E. Caldeweyher, S. Ehlert, A. Hansen, H. Neugebauer, S. Spicher, C. Bannwarth and S. Grimme, *J. Chem. Phys.*, 2019, **150**, 154122.
33 E. van Lenthe and E. J. Baerends, *J. Comput. Chem.*, 2003, **24**, 1142–1156.
34 T. Ziegler and A. Rauk, *Inorg. Chem.*, 1979, **18**, 1558–1565.
35 T. Ziegler and A. Rauk, *Inorg. Chem.*, 1979, **18**, 1755–1759.
36 F. Neese, *Wiley Interdiscip. Rev.: Comput. Mol. Sci.*, 2011, **2**, 73–78.
37 F. Neese, *Wiley Interdiscip. Rev.: Comput. Mol. Sci.*, 2017, **8**, e1327.
38 T. Noro, M. Sekiya and T. Koga, *Theor. Chem. Acc.*, 2013, **132**, 1363.
39 M. Barysz and A. J. Sadlej, *J. Mol. Struct. Theochem*, 2001, **573**, 181–200.
40 W. A. de Jong, R. J. Harrison and D. A. Dixon, *J. Chem. Phys.*, **2001**, 114, 48–53.
41 T. Lu and F. Chen, *J. Comput. Chem.*, 2012, **33**, 580–592.
42 M. A. Spackman and D. Jayatilaka, *CrystEngComm*, 2008, **11**, 19–32.
43 B. M. Otten, K. M. Melançon and M. A. Omary, *Comments Inorg. Chem.*, 2018, **38**, 1–35.
44 T. Lu and Q. Chen, *J. Comput. Chem.*, 2022, **43**, 539–555.
45 A. L. Chistyakov, I. V. Stankevich, N. P. Gambaryan, I. A. Tikhonova and V. B. Shur, *Russ. Chem. Bull.*, 1995, **44**, 997–1004.
46 H. V. R. Dias, S. A. Polach and Z. Wang, *J. Fluorine Chem.*, 2000, **103**, 163–169.
47 Z. Lu, A. Burini, R. N. McDougald, S. Ricci, L. Luciani, V. N. Nesterov, A. M. Rawashdeh, M. A. Omary and R. Galassi, *Eur. J. Inorg. Chem.*, 2022, **2022**, e202101056.
48 O. Elbjeirami, C. N. Burress, F. P. Gabbaï and M. A. Omary, *J. Phys. Chem. C*, 2007, **111**, 9522–9529.

